Optical vector network analyzer for single scan measurements of loss, group delay and polarization mode dispersion

Luna Technologies, 3157 State Street, Blacksburg, VA 24060
540.961.5190
www.lunatechnologies.com
support@lunatechnologies.com

May 17, 2005

1 Introduction

The Jones matrix (JM) or linear transfer function (TF) of a fiber-coupled component, when measured as a function of frequency, contains all of the information required to predict final component performance (loss, dispersion, polarization effects, etc...).[1] In this white paper we describe a novel interferometric technique for single-scan, high resolution spectral measurements of the TF of an optical component. In addition, we demonstrate mathematically how the TF is obtained from this measurement apparatus. We then show that highly accurate spectral amplitude and phase information can be extracted from the TF in the form of polarization-averaged group delay (GD), polarization mode dispersion (PMD), insertion loss (IL), and polarization dependent loss (PDL). Data is presented demonstrating greater than 100 dB, 80 dB and 60 dB dynamic range for the polarization-averaged IL, GD and PMD measurements, respectively. The elimination of the need for multiple wavelength scans in combination with the accurate and sensitive nature of the interferometric measurement technique yields an instrument ideally suited for high resolution metrology of passive optical components for high bit-rate network applications (e.g. tunable dispersion compensators, fiber Bragg gratings, arrayed waveguide gratings, etc.)

2 Optical network

The measurement technique is based on swept-wavelength interferometry (SWI). [2, 3, 4] The optical network used for single scan measurements of the TF is shown in Figure 1. A tunable laser source (TLS) is used in combination with concatenated

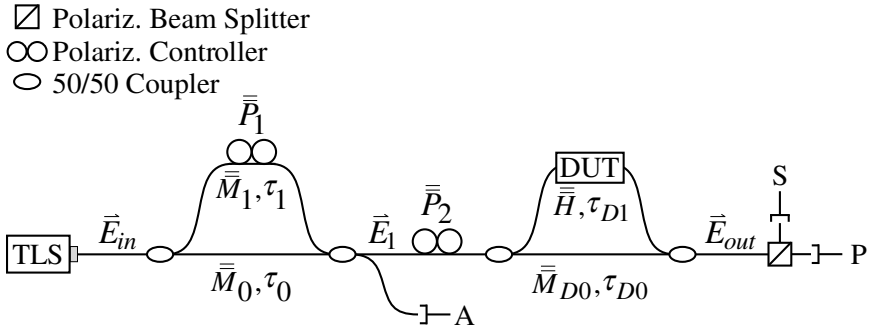

Figure 1: Optical vector network analyzer.

Mach-Zender interferometers, two polarization controllers, a polarization beam splitter and three photodiodes labelled "S," "P" and "A". The TLS used is capable of operating, mode-hop free, across the C and L communication bands with a specified line-width of 200 KHz. The laser was tuned at 70 nm/s. Not shown are a wavelength reference (HCN gas cell) and an auxiliary interferometer. The NIST-calibrated wavelength reference is used to adjust for wavelength errors in the start wavelength of a measurement scan. The auxiliary interferometer is used as a trigger to sample the incoming data at equal frequency increments. This serves to correct for deviations from linearity during laser tuning and thus enable proper application of the Fourier transform processing described in following paragraphs. The use of both a gas cell and an auxiliary interferometer are well-known methods to correct for phase errors during laser tuning.[5]

3 Theory

The interferometer on the left in Fig. 1 is used to create two time-shifted, orthogonal polarization states with which to simultaneously interrogate the DUT. Below we show that when this network is properly aligned it can be used to measure the TF of the DUT in a single laser scan. For the purposes of this analysis, we assume a normalized input laser field of the form $\vec{E}_{in} = \hat{\rho}\, e^{-i\omega t}$ where $\hat{\rho}$ is a unit vector describing the state of polarization and ω is the instantaneous optical frequency. After passing through the first Mach-Zehnder interferometer, the field can be described by

$$\begin{aligned} \vec{E}_1 &= (\bar{\bar{M}}_0 + \bar{\bar{M}}_1)\, \hat{\rho}\, e^{-i\omega t} \\ &= \hat{m}\, e^{-i\omega(t-\tau_0)} + \hat{n}\, e^{-i\omega(t-\tau_1)}. \end{aligned} \tag{1}$$

Here $\bar{\bar{M}}_0$ and $\bar{\bar{M}}_1$ are matrix operators that describe the propagation of the field through the two branches of the first interferometer, τ_0 and τ_1 are the delays associated with these branches, and $\hat{m}$ and $\hat{n}$ are two unit vectors describing the output states of polarization. The polarization controller, $\bar{\bar{P}}_1$, is used to modify the polarization

state of the field in the upper branch of the interferometer such that $\hat{m}$ and $\hat{n}$ are orthogonal. In practice, this orthogonality condition can be established by minimizing the fringe amplitude at the detector labeled "A" in Fig. 1.

The second polarization controller, $\bar{\bar{P}}_2$, is then used to ensure that, after passing through the lower branch of the second interferometer, the field components associated with the two branches of the first interferometer are divided equally between the orthogonal polarization states defined by the polarization beam splitter, $\hat{s}$ and $\hat{p}$. This condition is described by

$$\bar{\bar{M}}_{D0}\bar{\bar{P}}_2\hat{m} = \frac{1}{\sqrt{2}}(\hat{s}+\hat{p})\, e^{i\omega\tau_{D0}} \tag{2}$$

$$\bar{\bar{M}}_{D0}\bar{\bar{P}}_2\hat{n} = \frac{1}{\sqrt{2}}(\hat{s}-\hat{p})\, e^{i\omega\tau_{D0}}, \tag{3}$$

where $\bar{\bar{P}}_2$ is the TF of the second polarization controller, $\bar{\bar{M}}_{D0}$ is the matrix representing propagation through the lower branch of the second interferometer, and τ_{D0} is the delay associated with this branch. The field that propagates through the lower branch, termed the reference field, can then be written as

$$\begin{aligned}\vec{E}_{R,out} = \bar{\bar{M}}_{D0}\bar{\bar{P}}_2\vec{E}_1 = {} & \frac{1}{\sqrt{2}}(\hat{s}+\hat{p})\, e^{-i\omega(t-\tau_0-\tau_{D0})} \\ & + \frac{1}{\sqrt{2}}(\hat{s}-\hat{p})\, e^{-i\omega(t-\tau_1-\tau_{D0})}.\end{aligned} \tag{4}$$

The field that propagates through the upper branch of the second interferometer experiences a polarization dependent loss and phase shift due to the DUT which can be described by the DUT's TF, $\bar{\bar{H}}$. This field can be expressed as

$$\vec{E}_{D,out} = \bar{\bar{H}}\bar{\bar{P}}_2\hat{m}e^{-i\omega(t-\tau_0-\tau_{D1})} + \bar{\bar{H}}\bar{\bar{P}}_2\hat{n}e^{-i\omega(t-\tau_1-\tau_{D1})}, \tag{5}$$

where τ_{D1} is the delay associated with the upper branch of the second interferometer.

The polarization beam splitter then splits the combined field, $\vec{E}_{out}$, into two orthogonal components $\hat{s}$ and $\hat{p}$ according to

$$\begin{aligned}E_s\hat{s} = (\vec{E}_{out}\cdot\hat{s})\hat{s} = \{ & \frac{1}{\sqrt{2}}[e^{-i\omega(t-\tau_0-\tau_{D0})} + e^{-i\omega(t-\tau_1-\tau_{D0})}] \\ & + [(\bar{\bar{H}}\bar{\bar{P}}_2\hat{m})\cdot\hat{s}]e^{-i\omega(t-\tau_0-\tau_{D1})} \\ & + [(\bar{\bar{H}}\bar{\bar{P}}_2\hat{n})\cdot\hat{s}]e^{-i\omega(t-\tau_1-\tau_{D1})}\}\hat{s}\end{aligned} \tag{6}$$

$$\begin{aligned}E_p\hat{p} = (\vec{E}_{out}\cdot\hat{p})\hat{p} = \{ & \frac{1}{\sqrt{2}}[e^{-i\omega(t-\tau_0-\tau_{D0})} - e^{-i\omega(t-\tau_1-\tau_{D0})}] \\ & + [(\bar{\bar{H}}\bar{\bar{P}}_2\,\hat{m})\cdot\hat{p}\,]e^{-i\omega(t-\tau_0-\tau_{D1})} \\ & + [(\bar{\bar{H}}\bar{\bar{P}}_2\,\hat{n})\cdot\hat{p}\,]e^{-i\omega(t-\tau_1-\tau_{D1})}\}\hat{p}.\end{aligned} \tag{7}$$

It is important to note here that simple basis rotations applied to a TF have no effect on the linear parameters (GD, PMD, etc.) extracted from that TF. We can apply a unitary and invertible rotation matrix, $\bar{\bar{R}}$, and its inverse such that $\bar{\bar{H}}\bar{\bar{P}}_2 = \bar{\bar{H}}\bar{\bar{P}}_2\bar{\bar{R}}^{-1}\bar{\bar{R}}$. We then assume that the second polarization controller, $\bar{\bar{P}}_2$, is a simple rotation with negligible PMD such that $\bar{\bar{H}}\bar{\bar{P}}_2\bar{\bar{R}}^{-1} = \bar{\bar{H}}'$ is just a rotated version of the TF, $\bar{\bar{H}}$. This constitutes the only major assumption of this analysis and limits the smallest measurable PMD value to the residual PMD in the controller, $\bar{\bar{P}}_2$, which is typically on the order of 5 - 10 fs.

We can then choose $\bar{\bar{R}}$ so that $\bar{\bar{R}}\,\hat{m} = \hat{s}$ and $\bar{\bar{R}}\,\hat{n} = \hat{p}$, a simple operation of rotating one set of orthogonal vectors into another. For simplicity, we now introduce a new notation such that $H_{sp} = (\bar{\bar{H}}'\hat{s}\,)\cdot\hat{p}$. We also introduce two new variables $\tau = \tau_1 - \tau_0$ and $\tau_D = \tau_{D1} - \tau_{D0}$. Using this notation and doing some algebra, one can show that the intensities at the two detectors, S and P, can be written as:

$$I_p(\omega) = E_pE_p^* \propto Re[H_{pp}e^{i\omega(\tau_D+\tau)} - H_{sp}e^{i\omega(\tau_D-\tau)}] + \ldots \tag{8}$$

$$I_s(\omega) = E_sE_s^* \propto Re[H_{ps}e^{i\omega(\tau_D+\tau)} + H_{ss}e^{i\omega(\tau_D-\tau)}] + \ldots \tag{9}$$

In these equations, we have omitted several terms that do not relate directly to the extraction of the TF – specifically terms with no delay, with delay τ, and with delay τ_D. The four terms, H_{pp}, H_{sp}, H_{ps}, and H_{ss}, in Eqs. 8 and 9 are the four elements of the DUT TF (including the fiber pigtails and the polarization controller, $\bar{\bar{P}}_2$) expressed in the basis of the polarization beam splitter.

Examining Eqs. 8 and 9, one can see that as the TLS frequency is swept, fringes are generated as a function of time on the two detectors, S and P, at frequencies proportional to the delays $\tau_D + \tau$ and $\tau_D - \tau$. A discrete Fourier transform (FFT) of the data from each channel will reveal impulses at these delays. Three such impulses are shown in Figure 2. This plot diplays the FFT of raw data from one of the two detectors, S or P. The DUT in this case was a Bragg grating. The impulses at $\tau_D - \tau$ and $\tau_D + \tau$ are associated with two elements of the DUT TF.

The four impulses associated with the TF of the DUT (two from each detector) can be extracted by the process of bandpass filtering these four impulses and transforming them individually back to the optical frequency domain. The dashed-line boxes in Fig. 2 represent bandpass filters used to extract the two impulses associated with the DUT TF. This digital filtering process yields the four complex TF elements.

Any dispersiveness in the DUT causes the impulses associated with the TF elements to spread in time. This is well illustrated by the spreading of the Bragg grating impulses shown in Fig. 2. The delay difference, $\tau = \tau_1 - \tau_0$, must therefore be chosen such that the spreading does not cause the peaks to overlap in time. Such an overlap renders the TF elements "mixed" in the time domain and the process of filtering

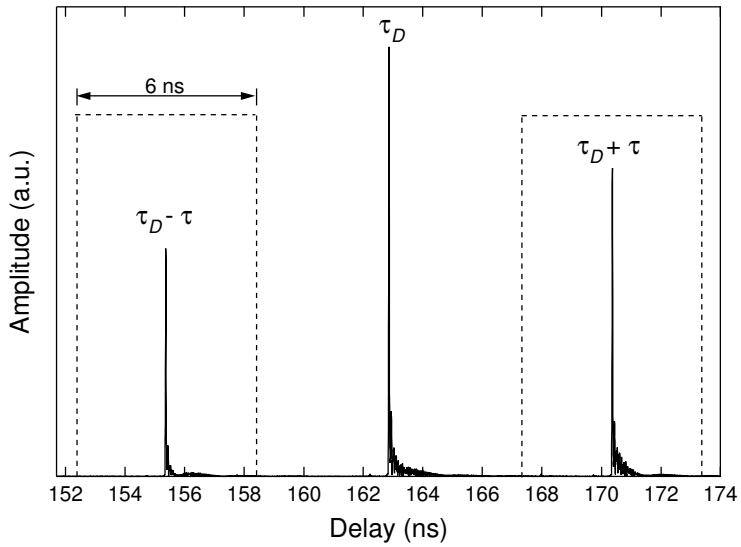

Figure 2: Discrete Fourier transform of raw data from one of the two detectors, S and P. The DUT was a Bragg grating. The peaks at $\tau_D - \tau$ and $\tau_D + \tau$ are associated with two elements of the DUT TF. The dashed boxes represent bandpass filters used to "slice out" these impulses in order to extract the DUT TF elements. The 6 ns width of these filters limits the measurable GD or PMD to 6 ns.

individual peaks becomes impossible. In this work, a delay of about 6 ns was used. This value limits the measurable GD and PMD ranges to 6 ns and, because of the Fourier transform relationship between time duration and frequency resolution, the effective wavelength resolution of the measurement to ~ 1.5 pm.

The delay difference in the interferometer used for triggered acquisition, τ_t, limits the delay of the DUT to no greater than $\tau_t/2$. The maximum τ_t is, in turn, limited by the scan speed of the laser and the sampling speed of the data acquisition system used. For a current embodiment of the measurement system, DUT lengths are limited to < 100 m in transmission and half that length in reflection.

4 Results

Figure 3 shows the GD of an acetylene gas cell absorption line as measured using the technique described above. It is important to note here that a simple definition of GD as the derivative of the phase with respect to frequency yields a quantity that varies as a function of input polarization state. When quantifying "the" GD of a component, then, it is preferable to calculate some average GD with respect to polarization state. One common method to define an average GD is to find the GD associated with the principle states of polarization[7] and average these two results[2]. We find that this formulation yields a GD that becomes ill-defined for components with high Polarization Dependent Loss (PDL). Rather than use this definition, then,

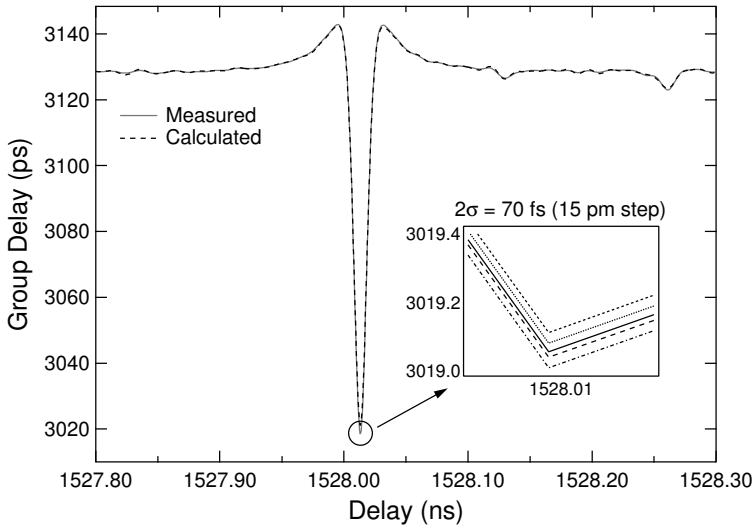

Figure 3: Group delay of an Acetylene gas cell as measured (solid) using the technique described in this paper and as calculated (dashed) from the loss of the same cell. The inset shows five representative data sets illustrating measurement repeatability.

we apply a weighted average phase derivative to calculate the GD from the measured TF:

$$GD(\omega) = \frac{arg\left\{\sum H_{ij}(\omega)\, H_{ij}^{*}(\omega - \Delta\omega)\right\}}{\Delta\omega}, \tag{10}$$

where the sum is over the four matrix elements. This definition weights transmitting states more heavily than non-transmitting and thus yields correct polarization averaged results, even for components with non-transmitting states (eg. a polarizer).

In order to demonstrate the precision of the GD measurement, 20 data sets with 32 scans averaged per set were recorded and compared. Each individual data set took less than 0.5 seconds to acquire. These data were taken using a 1.5 pm wavelength step. At the minimum of the absorption line the 2σ variation of the GD was found to be 70 fs with a 15 pm derivative step size and 40 fs with a 30 pm step. These step sizes were chosen as they are most relevant to metrology of components for narrowband, high bit-rate systems. The inset in Fig. 3 shows a representative subset of these data with a 15 pm step size. In order to check the accuracy of the GD measurement, we applied the Kramers-Kronig relationships to derive the GD from the measured loss through the gas cell[6]. The calculated GD, shown as the dotted line in Fig. 3, closely matches the measured GD. Note that the insertion loss of the gas cell was also measured with the technique described herein.

Given $\bar{\bar{H}}(\omega)$, the differential group delay (DGD), or polarization mode dispersion (PMD) [where DGD = PMD] is calculated by finding the eigenvectors of $[d\bar{\bar{H}}/d\omega]\bar{\bar{H}}^{-1}$, which correspond to the principle states of polarization (PSP's) of the DUT.[7] The

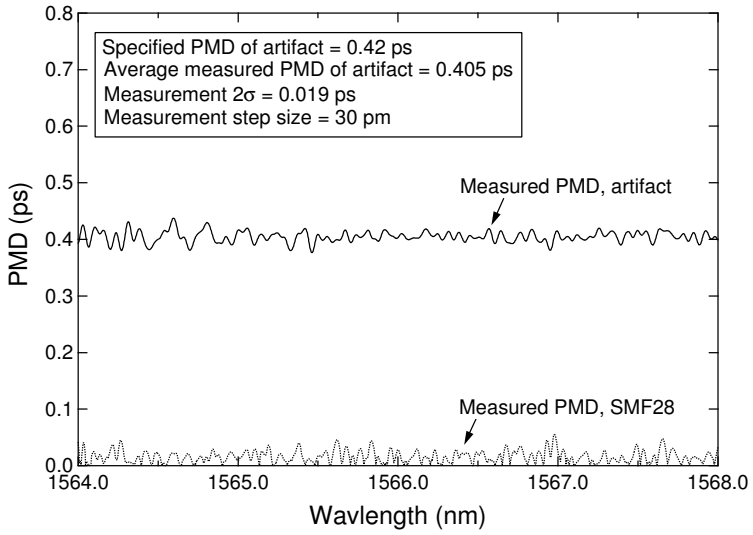

Figure 4: Measured PMD of a PMD artifact (solid) and a 7m length of SMF28 fiber (dotted) using the network shown in Fig. 1.

imaginary parts of the eigenvalues of the product $[d\bar{\bar{H}}/d\omega]\bar{\bar{H}}^{-1}$ are the group delays associated with the two PSP's. If ρ_1 and ρ_2 denote the two eigenvalues, then the PMD, $\Delta\tau$, is given by

$$\Delta\tau = \mathrm{Im}[\rho_1 - \rho_2]. \tag{11}$$

A measurement of the PMD of a calibrated artifact is shown in Fig. 4. While the PMD value quoted by the manufacturer of the artifact is 0.42 ps, we measure an average PMD across the wavelength range of the scan of 0.405 ps with a standard deviation of 0.01 ps. The small difference is well within the expected measurement error. In order to further verify the accuracy of the PMD measurement, we measured the PMD of a 7 m length of SMF28 fiber. As is expected for this fiber, the measurement shows little PMD across the wavelength range of the scan (see Fig. 4). The standard deviation of this data set is, again, 0.01 ps. Both of these measurements were made using a 1.5 pm step and 30 pm smoothing and derivative step. Each measurement took less than a minute to acquire. For a step of 500 pm, the average measured PMD for the fiber is 8 fs, showing that the residual PMD of the measurement network is very small.

The coherent interferometric technique is ideal for metrology of narrow-band DWDM components that may have wavelength dependent loss features. To demonstrate this, we measured the TF of one channel of a fiber-coupled thin film filter designed as a wavelength multiplexer. Figure 5 shows the GD and PMD derived from the measured TF of this filter. The maximum and minimum insertion loss (IL) as a function of wavelength, measured with the same technique, are also shown. The two IL curves shown in Fig. 5, IL_{min} and IL_{max}, were generated numerically using

the TF by calculating the eigenvalues of $\bar{\bar{H}}\bar{\bar{H}}^{\dagger}$.[8] For this component, the minimum and maximum are nearly identical across the pass band of the device, indicating low PDL. One can see from Fig. 5 that IL features are resolvable down to less than -100 dB. In addition the GD and PMD are measurable at IL values down to -80 dB, demonstrating that this measurement technique enables dispersion characterization for components with very high loss.

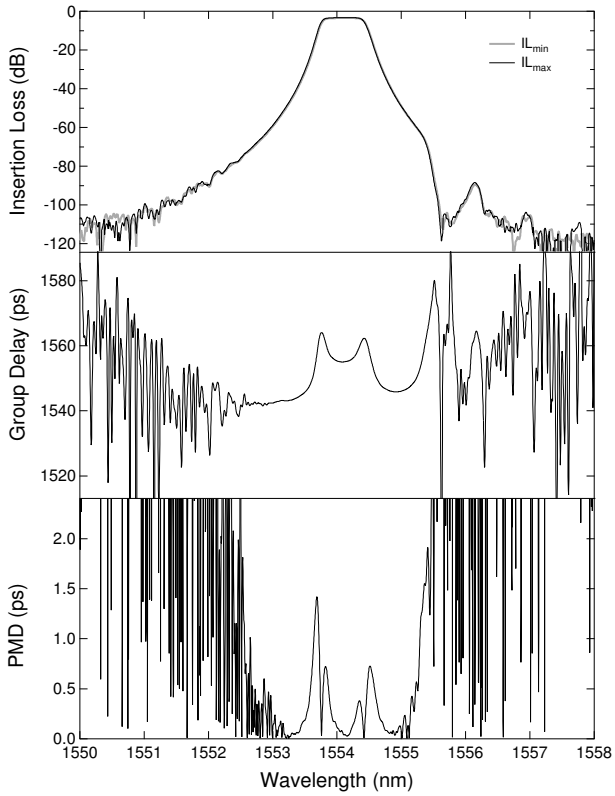

Figure 5: Measured IL, GD and PMD of a thin film filter using the network shown in Fig. 1. The two IL curves represent the maximum and minimum IL as a function of input polarization state and wavelength.

The high dynamic range achieved in this work is enabled first by the high sensitivity inherent in the homodyne interferometric technique used and second by careful averaging of multiple data sets. The averaging algorithm used first aligns the relative phases of each data set and then computes the mean of the complex data sets by averaging real and imaginary parts. This ensures that small contributions from noise in both amplitude and phase average to zero. If, instead, the amplitude and phase are averaged, as is more common, noise contributions average to a small, but non-zero, number. This averaging method, then, allows improved access to the full sensitivity of the measurement technique, thereby enabling the high levels of dynamic range reported above.

5 Conclusion

In this paper, we have concentrated on results for GD and PMD and IL. Other quantities, such as chromatic dispersion, PDL, and second-order PMD, are easily calculated from the TF as well. Also, via use of a Fourier transform, one can easily examine the behavior of the DUT in the optical time domain. While we have concentrated on transmission devices in this paper, the technique is easily adaptable to reflection devices by the addition of an optical switch downstream of the DUT. The single scan, accurate, and high dynamic range measurements yielded by this technique make it ideal for rapid, high-resolution characterization of passive optical components.

References

[1] The linear transfer function is the two-by-two matrix, $\bar{\bar{H}}(\omega)$, that relates the input and output electric field vectors of an optical system in the spectral domain according to $\vec{E}_{out}(\omega) = \bar{\bar{H}}(\omega)\vec{E_{in}}(\omega)$. We use the "transfer function" nomenclature because whereas the Jones matrix describes only the transfer of the polarization state, the transfer function also contains the average loss (insertion loss) and phase (chromatic dispersion).

[2] G. D. VanWiggeren, A. R. Motamedi, D. M. Baney, "Single-scan interferometric Component Analyzer," IEEE Photonics Technology Letters. **15** 263–265 (2003).

[3] U. Glombitza and E. Brinkmeyer, "Coherent frequency domain reflectometry for characterization of single-mode integrated optical waveguides," J. Lightwave Technol. **11** 1377–1384 (1993).

[4] M. Froggatt, T. Erdogan, J. Moore, and S. Shenk, "Optical frequency domain characterization (OFDC) of dispersion in optical fiber Bragg gratings," in *Bragg Gratings, Photosensitivity, and Poling in Glass Waveguides,* OSA Technical Digest Series (Optical Society of America, Washington, DC, 1999), paper FF2.

[5] R. Passy, N. Gisin, J. P. von der Wide and H. H. Gilden, "Experimental and theoretical investigations of coherent OFDR with semiconductor laser sources," J. Lightwave Technol. **12** 1622–1630 (1994).

[6] A. Motamedi, B. Szafraniec, P. Robrish and D. M. Baney, "Group delay reference artifact based on molecular gas absorption," in *Optical Fiber Communication,* OSA Technical Digest Series (Optical Society of America, Washington, DC, 2001), paper ThC8-1.

[7] B.L. Heffner, "Automated measurement of polarization mode dispersion and using Jones matrix eigenanalysis," IEEE Photon. Technol. Lett. **4** 1066-1069 (1992).

[8] B.L. Heffner, "Deterministic, analytically complete measurement of polarization dependent transmission through optical devices," IEEE Photon. Technol. Lett. **4** 451-454 (1992).